The Geographic Base

Journal Homepage: https://www.ngssnepal.org/journal

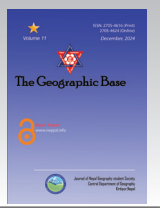

Estimation of Evapotranspiration over the Agricultural areas of Southeastern Nepal using Temperature-Vegetation Index Space Method

Shyam Krishna Karki[1,3], Weiqiang Ma[1,2*], Til Prasad Pangali Sharma[4]

[1]Institute of Tibetan Plateau Research, Chinese Academy of Sciences, Beijing 100085, China.
[2]Center for Excellence in Tibetan Plateau Earth Sciences, Chinese Academy of Sciences, Beijing 100085, China.
[3]University of Chinese Academy of Sciences, Beijing 100049, China.
[4]Nepal Mountain Academy, Tribhuvan University, Kathmandu, Nepal.
*** Corresponding author**: wqma@itpcas.ac.cn

Article info

Keywords: *evapotranspiration, NDVI, net radiation, water stress, remote sensing*

Received: 22nd Aug. 2024

Accepted: 20th Nov. 2024

DOI: https://doi.org/10.3126/tgb.v11i01.88625

Abstract

Nepal is characterized by remarkable physiographic diversity, which poses highly productive agricultural land across its southern plains stretching from east to west. However, limited precipitation and a declining trend in agricultural productivity has made accurate evapotranspiration (ET) estimation increasingly important, particularly during the dry season. This study presents an alternative approach the temperature-vegetation index T-VI space method for estimating ET with higher accuracy compared to previous studies that used different techniques. The root mean square error (RMSE) and mean absolute percentage error (MAPE) for daily ET (hourly ET) were 0.469 mm d^{-1} (0.09 mm h^{-1}) and 15.29% (15.45%) respectively. The high-resolution ET estimates (30m) obtained in this research, demonstrate that the T-VI space method is applicable in Nepal, providing valuable insights into regional hydrological processes, water stress patterns, and drought conditions within a single analytical framework. The findings offer

practical benefits for local farmers and government agencies for supporting future agricultural planning and promoting the efficient use of irrigation water.

Introduction

Evapotranspiration (ET) is the process of converting water to vapor from the open water surface, soil surface, and vegetation. ET is the most common and essential factor. Accurate ET estimation has become necessary to arid and semi-arid regions (Yamazaki et al. 2011). Water scarcity in those areas is increasing day by day due to climate change, resulting in a challenging task to estimate irrigation water requirements, hence planning and scheduling future irrigation schemes (Oki and Kanae 2006). However, ET is considered as one of the significant components for the hydrological cycle; only around 60-65% of precipitation water on land is transmitted back to the atmosphere through ET while the remaining portion gets able to meet oceans and inland seas by river networks (Yamazaki et al. 2011; Oki and Kanae 2006).

Many research have been done to enrich our understanding of land surface ET over the cropland in a regional scale and hence different methods used to estimate it (Allen et al. 1998; Courault et al. 2005; Allen et al. 2004; Ghorbani et al. 2015). Usually, ground data-based methods were used to estimate ET in the local region depending upon data availability, like the eddy covariance method, the Hargreaves method, and the Priestley-Taylor method (Saitta et al. 2020; Hargreaves and Samani 1985; Priestley and Taylor 1972). However, to cover large-scale areas, the remote sensing technique has become one of the most convenient approaches for actual ET estimation with the use of remotely sensed data, to cover a large area, however researchers have focused small geographical scale using high-resolution data (MacDonald et al. 1975; Gordon 1980; Mokhtari et al. 2019).

This research has covered a agricultural region of Southeastern Nepal, where more than 60% of the total population depend directly on agriculture for their daily living (Paudel 2016; Menon 2009). Accurate ET estimation to address agricultural water requirements and balance the local hydrological cycle has become crucial for Nepal. During the dry season, mainly from October to March, the primary winter production in the region is Wheat, and its production mainly depends upon the precipitation and local water level (Menon 2009; Devkota and Phuyal 2016). Droughts are increasing, and the precipitation extremities has observed due to climate change, that significantly during the wheat production period in Southeastern Nepal (Hamal et al. 2020; Subba et al. 2019). As a combined effect of climatic changes, wheat production has decreased due to water scarcity during the winter season (Hamal et al. 2020; Devkota and Phuyal 2016), making accurate ET estimation

over cropland play a very decisive role in balancing irrigation water requirement.

Many studies have used residual method and graphical approach to retrieve (Choudhury et al. 1994; Price 1990; Jiang and Islam 2001). The methods that are based on residual concept use the value leftover after subtracting sensible heat flux (H) and soil heat flux (G) from net radiation flux (R_n). This residual term is then considered as latent heat flux (LET or LE) which later used to calculate daily, monthly or seasonal ET (Bastiaanssen W.G.M. et al. 1998; Reyes-gonz et al. 2019). Based on scatter plots between Land surface temperature (LST) and normal difference vegetation index (NDVI) or sometimes simply vegetation index, a second group makes it to refer as graphical method or graphical approach. This method is firstly proposed by Price (1990) and later used successfully by many researchers to estimate and understand ET (Jiang and Islam 2001; Pérez et al. 2017; Zhu et al. 2020; Huang et al. 2020). In this approach, three different geometrical shapes (mainly triangular, rectangular, and trapezoidal) are used, relying on the concept of the upper and lower limit of evaporative fraction (Tang et al. 2010; Garcia et al. 2014; Pérez et al. 2017). With less intricacy and fewer variables compared to other methods, this approach valid for equitable estimation of evaporative fraction (EF) and hence ET (Batra et al. 2006; Minacapilli et al. 2016). Many past and recent researches have shown trapezoidal shape among three as the most reliable, popular, and valuable approach to estimate ET with the least possible error (Pérez et al. 2017; Zhu et al. 2020; Huang et al. 2020). Usually, the latent heat flux using graphical approach can be estimated by modifying Priestly Taylor (PT) equation for wet areal evaporation (Priestley and Taylor 1972) as:

$$ET = \left[\frac{\Delta}{\Delta + \gamma}\right](R_n - G) \qquad (1)$$

Where, γ is Priestley-Taylor coefficient (PT_c) and is dimensionless, Δis saturation vapor pressure, R_n is net radiation and G is soil heat flux.

The graphical approach is useful to accurately evaluate the actual ET from remote sensing data. However, research has shown that it has some drawbacks about selecting hot and cold pixels very accurately (Long and Singh 2013; Bastiaanssen et al. 2010), making it quite challenging to estimate the dry and wet limitation evaporation calculation validly. Therefore, being very challenging for researchers to reckon the precise value of evaporative fraction (EF), it is always foremost to evaluate each variable used in estimation meticulously. Since this paper has remote sensing data, the graphical approach been used. EF estimation using remote sensing data based on a graphical approach mainly depends upon two variables, vegetation index (VI) and land surface temperature (LST) (Sun 2016; Choi and Qu 2017). The concept proposed and used initially

by (Tang et al. 2010) for EF estimation is a universally used method to assess EF using remote sensing data. We need to define and calculate the dry limit and wet limit separately, implementing the idea of zero evaporation at the zone with no vegetation and highest LST to the maximum evaporation at the area with higher vegetation cover and lowest LST.

This research aims to estimate and validate the hourly, daily, and monthly ET retrieved from remote sensing data using the least possible variables. To evaluate the evaporative fraction's dry and wet limits, trapezoidal graphical shape analysis based on land surface temperature (LST) and normalized difference vegetation index (NDVI) obtained using remote sensing data was used. In addition to that, the temperature-vegetation index space method have been used for the first time in Nepal's case. This alternative approach for ET estimation could play a vital role in obtaining the ET results from remote sensing data with higher accuracy. With these outputs and results, this research hopes to help local farmers, government and policy makers for the scientific use of irrigation water amount in the dry season in Nepal.

Methods and Materials

Study area

This paper covers the Southeastern part of Nepal. It stretches from 26°22′ to 27°05′ N and 85°32′ to 88°12′ E. This study area covers a small but crucial region of Nepal. For this study, two Landsat images with path 140 row 041 and path 140 row 042, were used, as shown in Figure 1.

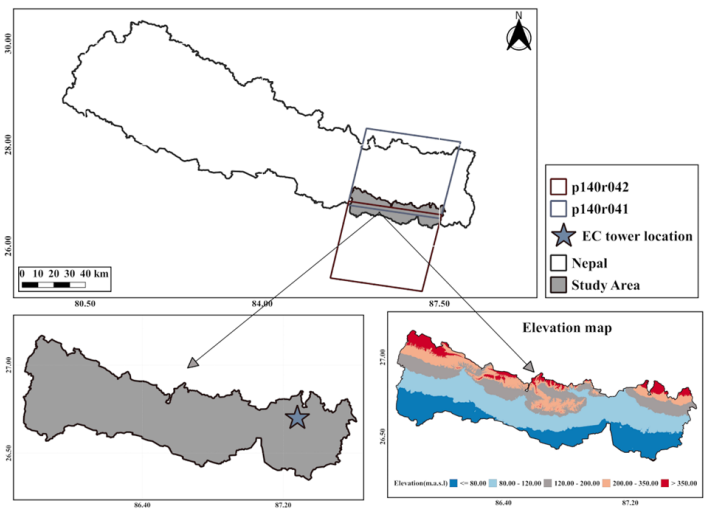

Figure 1. Study area representing southeastern areas of Nepal with location of EC flux tower station and the elevation variation within the study area.

This study area was selected because of its importance in agriculture and the availability of ground truth value over agricultural area as well as to keep elevation range within 60 m to 360 m (a.s.l) as far as possible using the DEM map of Nepal. Two different Landsat images have been selected because both images cover the EC flux tower's location as their common overlapping area.

The land cover is mainly dominated by agricultural areas, whereas some portions are also covered by forest, water bodies, and barren land. Paddy from June to October, Wheat from October to March, and Maize from March to June are the main crop rotations throughout the year (Shrestha et al. 2013). This study area's climate pattern is classified as subtropical savannah using Köppen Geiger's climatic classification scheme (Karki et al., 2016).

Data

Remote sensing data

To estimate land surface temperature (LST), hourly ET, daily ET, and monthly ET, it has used four different Landsat-8 images collection 1, level 1 for the year 2016. Required images were downloaded from the USGS official website (https://earthexplorer.usgs.gov/), free of cost for the research purpose. To cover Nepal's southeastern agricultural areas and to analyze different climatic parameters, 18 Landsat-8 images for 9 different days of the year 2016 were used. The details of the Landsat-8 images used in this study.

Other data

Data and results obtained from one EC flux tower data located in Tarahara, 26°42′ N and 88°16′ were used to validate the results obtained through Landsat-8 images. It was the first EC flux tower established in Nepal by a joint effort from the Institute of Tibetan Plateau of Research, Chinese Academy of Sciences (ITP-CAS), and Tribhuvan University (TU) Nepal with an elevation of 120 m a.s.l. Besides EC flux tower data, we used the Advanced Spaceborne Thermal Emission and Reflection (ASTER) Digital Elevation Model (DEM) map with latitude and longitude information to estimate the net radiation.

Table 1. Details of the Landsat-8 images used in this study

Path	Rows	Dates of satellite images
140	041	February 5 and 21, March 8 and 24, April 9 and 25, October 18, November 3 and 19
140	042	February 5 and 21, March 8 and 24, April 9 and 25, October 18, November 3 and 19

Table 2. Average value of different intermediate results calculated during the process of daily ET estimation.

DOY	Average EF	Average Rn ($W\ m^{-2}$)	Average G ($W\ m^{-2}$)	Average ETinst ($mm\ h^{-1}$)
36	0.53	222.17	24.81	0.16
52	0.61	306.57	29.22	0.26
68	0.57	580.72	60.71	0.43
84	0.54	624.67	68.49	0.44
100	0.58	603.45	61.49	0.49
116	0.57	536.61	55.57	0.59
292	0.72	589.23	42.54	0.57
308	0.77	456.65	27.38	0.49
324	0.62	415.38	38.74	0.35

Here, DOY stands for day of the year, EF for evaporative fraction, Rn for net radiation in watts per square meter ($W\ m^{-2}$), G for soil heat flux in watt per square meter ($W\ m^{-2}$), and Etinst for instantaneous evapotranspiration in millimeters per hour ($mm\ h^{-1}$).

Data process

Initially, all the Landsat-8 images were pre-processed using the QGIS SCP plugin for the radiometric and atmospheric correction. For the cloud masking, cloud contamination was checked using QGIS and f-mask from MATLAB. After pre-processing, band 5 and band 4 from the images were used for NDVI calculation. Later NDVI was used to compute vegetation fraction and land surface emissivity. After that, we computed land surface temperature using the concept from (Jimenez-Munoz et al. 2009) as:

$$T_S = \gamma \left[\frac{1}{\varepsilon}(\Psi_1 L_{sen} + \Psi_2) + \Psi_3\right] + \delta \quad (2)$$

Where T_S is the LST, γ and δ are the psychrometric, ε is the land surface emissivity, Ψ_1, Ψ_2 and Ψ_3 are three atmospheric function parameter and L_{sen} is bright sensor temperature.

EF Retrieval

For the estimation of EF, NDVI, and temperature results obtained from Landsat-8 images were used. In this research, a trapezoidal shape, relying on the relation of temperature to vegetation-

index (T-VI) was implemented. For the determination of dry edge and wet edge related to the trapezoidal shape, a concept proposed by Hu et al. (2019) with a tiny modification was used. To find out the dry and wet edge of trapezoidal shape, the steps followed were as described below:

1) Firstly, NDVI values should be divided into M even intervals (20 intervals in this study).

2) Secondly, each NDVI interval should be divided into N sub-intervals. The value of N can be 5 or more than 5 (5 in our case).

3) After dividing to N sub-intervals, average temperature (Tavg) and standard deviation (∫) were computed for each subinterval.

4) LST values greater than the Tavg plus four times ∫ were considered spurious pixels and hence discarded. This was used later for the determination of dry edge. Similarly, in the case of wet edge, LST values that are lower or smaller than the Tavg minus four times ∫ were discarded.

5) After discarding spurious pixels, maximum and minimum LST values for each sub-interval were noted down so that each interval has five different maximum LST and minimum LST values.

6) Average of maximum LST values $(T_{min})_{avg}$ and standard deviation (∫) were determined for each sub-interval. A similar process is followed for minimum LST values.

7) If the maximum and minimum LST of each sub-interval was less than $(T_{max})_{avg}$ or $(T_{min})_{avg}$ minus ∫, then such sub-intervals were discarded to find new T_{avg}.

8) Step 7 is followed again if there were sub-intervals that need to be discarded. After discarding all the abnormal sub-intervals, maximum and minimum representative LST values were calculated for each interval, which can be obtained from the average of LST values from remaining sub-intervals.

9) After assigning maximum and minimum LST values for each interval, its linear regression with NDVI was used to get the root mean square error (RMSE).

10) To find out and discard the abnormal intervals, intervals with LST values less than T (from linear regression) minus 2 times RMSE were excluded.

11) The remaining maximum LST for each interval represents the maximum end members, while that of minimum LST represents the minimum end members.

12) A linear least square regression between the maximum end members was used for dry edge. Similarly, the wet edge was determined using minimum end members.

The EF from trapezoidal shape is calculated as:

$$EF = \Phi\left[\frac{\Delta}{\Delta+\gamma}\right] \quad \text{.....(3)}$$

where Φ is a combined-effect parameter which is the reason for aerodynamic resistance, it is calculated by following the concept from (Tang et al. 2010).

After that, we computed the latent heat flux (LE) using a modified form of equation (1) as used by (Jiang and Islam 2001) for remote sensing data as:

$$LE = ET = \Phi\left[\frac{\Delta}{\Delta+\gamma}\right](R_n - G) \quad \text{.....(4)}$$

R_n was acquired following the similar concept in (Allen et al. 2007) as:

$$R_n = (1 - \alpha)R_{S\downarrow} + R_{L\downarrow} - R_{L\uparrow} - (1-\varepsilon_0)R_{L\downarrow} \quad \text{.....(3)}$$

where α is a dimensionless parameter called surface albedo and is calculated using the modified idea proposed using Landsat-8 images by Oh et al. (2020). Other parameters $R_{S\downarrow}$, $R_{L\downarrow}$ and $R_{L\uparrow}$ represent the downward shortwave, downward longwave and upward longwave radiation respectively. These radiations and broadband surface emissivity ε_0 were calculated in a similar manner as Allen et al. (2007) or Madugundu et al. (2017). Adding the value of net radiation to EF, ground heat flux (G) was estimated as (Tanguy et al. 2012; Brutsaert 1998):

$$\beta = \frac{G}{R_n} \quad \text{..... (6)}$$

where β is EF based parameter and is given as;

$$\beta = a + b.EF \quad \text{..... (7)}$$

with a = 0.23 and b = -0.22. After determining LE, instantaneous ET (ET_{inst}) at the time of satellite overpass ($mm\ h^{-1}$) is computed by taking the concept from Allen et al. (2007) as:

$$ET_{inst} = 3{,}600\left(\frac{LE}{\lambda\rho_w}\right) \quad \text{..... (8)}$$

where, 3600 is used for time conversion from seconds to an hour. λ is the latent heat of vaporization ($J\,Kg^{-1}$). ρ_w is the density of water which is 1000 Kg m^{-3}. After computation of ET_{inst}, we calculated reference ET fraction (ET_rF) as:

$$ET_rF = \frac{ET_{inst}}{ET_r} \quad \text{..... (9)}$$

All the ET parameters here in $mm^{h^{-1}}$. Here ET_r represents reference mean ET from EC flux tower data, which can be obtained using the concept from Walter et al. (2004). Daily ET (ET_{24}), was calculated by using ET_rF taking the concept form Allen et al. (2007) as:

$$ET_{24} = ET_rF.ET_{r24} \quad \text{..... (10)}$$

Where ET_{r24} is the daily ET from station data.

Error analysis

To test the performance accuracy of the method used in this study, two error analyses were done as:

Root mean square error (RMSE):

$$RMSE = \sqrt{\frac{\sum_{i=1}^{n} (E_i - O_i)^2}{n}} \quad \text{..... (11)}$$

Mean absolute percentage error (MAPE):

$$MAPE = \frac{100}{\underline{O}}\left(\frac{1}{n}\sum_{i=1}^{n} |E_i - O_i|\right) \quad \text{.... (12)}$$

Where E_i and O_i are representing estimated and observed results. The mean va'ıe of observed results is represented by $\underline{O}$ and number of results by n.

Results and Discussion

Evaporative fraction

Firstly, we computed NDVI and LST using Landsat-8 images. Using the obtained values of NDVI and LST, trapezoidal space shapes were plotted to calculate evaporative fractions for 9 different dates of 2016. Mean values of obtained NDVI, and EF are shown in Table 2. Estimated LST used for space method analysis were compared against the observed LST, which was calculated using longwave radiations from EC flux tower data. The RMSE and MAPE for estimated LST were 2.15 °C and 6.10%, respectively. Estimated LST used for space method analysis were compared against the observed LST, which was calculated using longwave radiations from EC flux tower data, as shown in Figure 2.

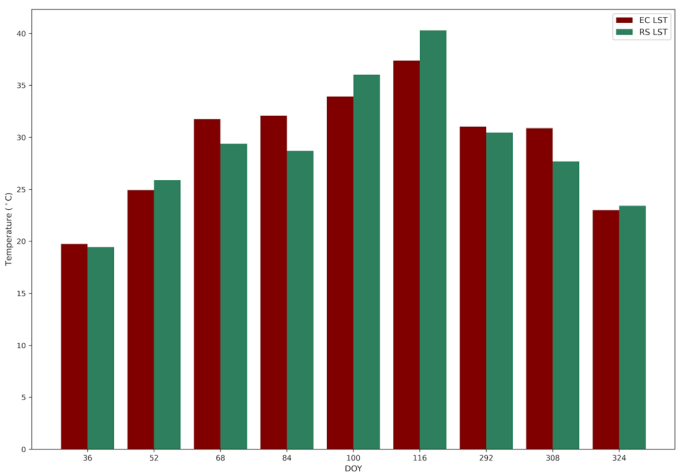

Figure 2. Comparison of estimated LST using Landsat-8 images with the observed LST from EC flux tower calculated using longwave radiations for nine different days of the year (DOY) 2016.

The RMSE and MAPE for estimated LST were 2.15 °C and 6.10%, respectively. Calculated NDVI and LST scatterly plotted against each other to determine the dry edge and wet edge. Trapezoidal graphical shape based on T-VI space method are shown in Figure 3.

Evapotranspiration

After calculating evaporative fraction, we calculated instantaneous ET and hence daily ET. As an intermediate product, we computed net radiation using the DEM method. Some of the intermediate results like the mean net radiation, ground heat flux, and latent heat flux are shown in Table 1. Net radiation results were compared against the observed net radiation results from the EC flux tower, and the RMSE and MAPE obtained for estimated results were 107.98 W m^{-2} and 19.72%, respectively. Using all required preliminary results, reference ET or instantaneous ET for nine different days of the year 2016 were obtained with the RMSE and MAPE of 0.09 mm h^{-1} and 15.45%, respectively, as shown in Figure 5.

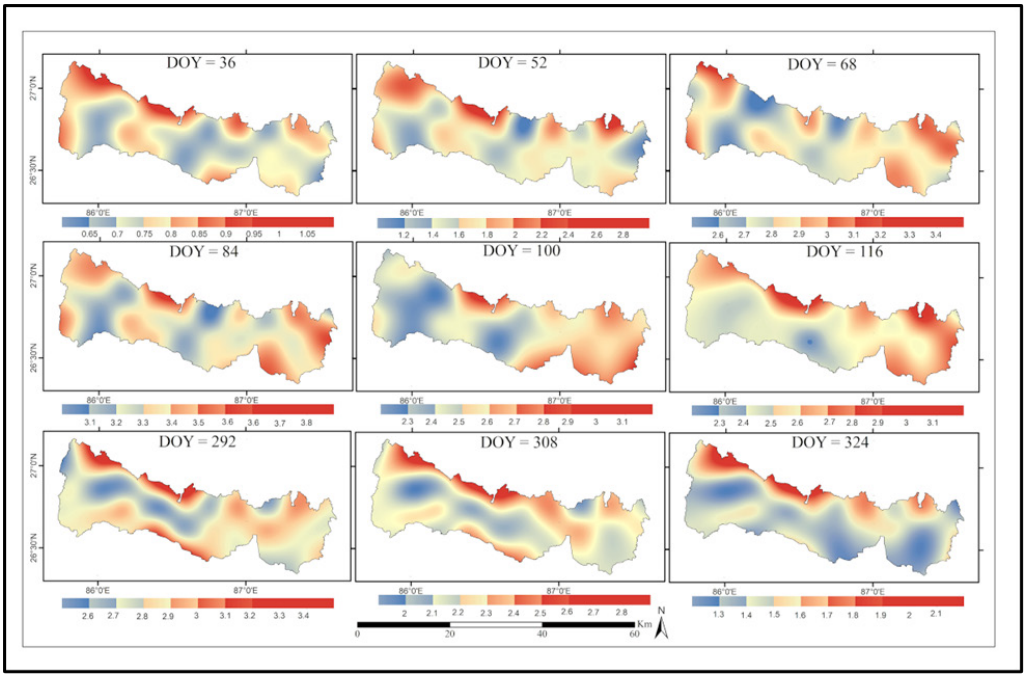

Figure 3. The spatial variation of daily ET based on T-VI space method using Landsat-8 images for nine different days of the year (DOY) 2016.

Mean instantaneous evapotranspiration for days 36, 52, 68, 84, 100, 116, 292, 308 and 324 are 0.16, 0.26, 0.43, 0.44, 0.49, 0.59, 0.57, 0.49 and 0.35 mm h^{-1} respectively. After instantaneous ET was computed and validated, we used them along with reference ET from EC flux tower data to estimate the daily ET results. The spatial variation of daily ET for nine different days of 2016 is shown in Figure 4**.** The mean estimated daily ET results had the RMSE and MAPE of 0.46 mm d^{-1} and 15.29%, respectively. The mean daily ET results estimated using Landsat-8 images and observed daily results are shown in Figure 5**.**

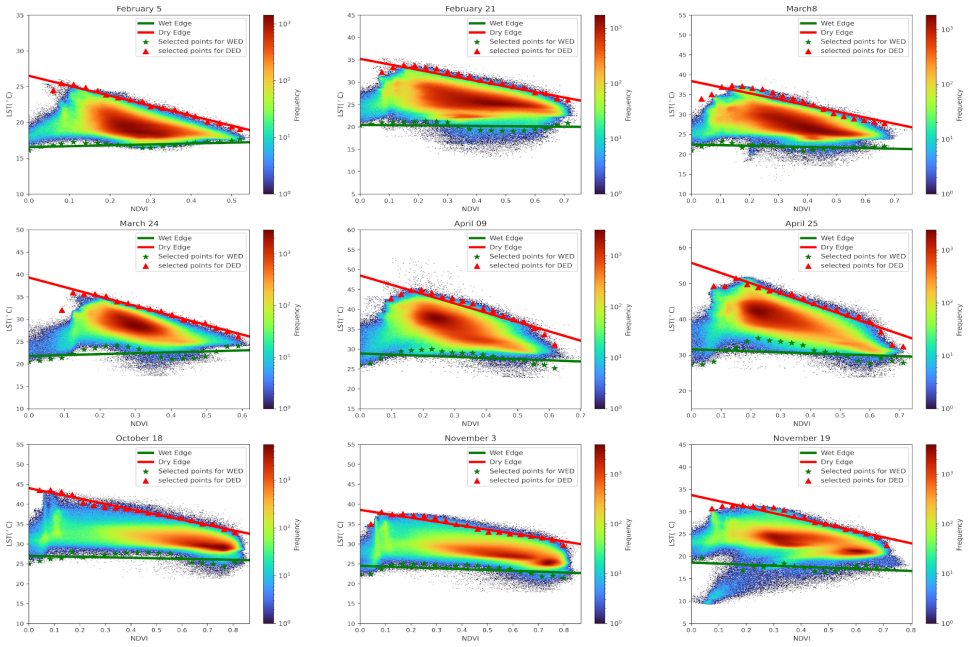

Figure 4. Trapezoidal shape based on T-VI space relationship from the scatter plot of NDVI and LST obtained using Landsat-8 images. Red stars and red line represent the dry edge determination (DED) points and dry edge while green stars and greenline represents wet edge determination (WED) points and wet edge for nine different dates.

It has computed and compared the estimated results for LST, net radiation, instantaneous ET, and daily ET. Results and errors presented in the results sections have shown the good performance of the T-VI space method used in this study. Errors in estimated results were comparable with other similar past results. The error in estimated LST using the single-channel method in this study

was close to the errors obtained in Yu et al. (2014); García-Santos et al. (2018) and Cristóbal et al. (2018). Estimated net radiation in this study compared with observed ground truth values, found to be in close agreement, and error was comparable with the error obtained in Pérez et al. (2017). The error in estimated net radiation might be because of some assumptions that we made during this research. We tried to maintain the study area's topography with the lowest elevation variation as far as possible and considered it a flat horizontal area. We use the flat horizontal area's concept during net radiation calculation despite having certain elevation variations, which might have brought some errors in estimated results. While choosing the study area, we also have to keep in mind that it is enough to provide a wide range of temperature variations that can be plotted against VI for EF computation.

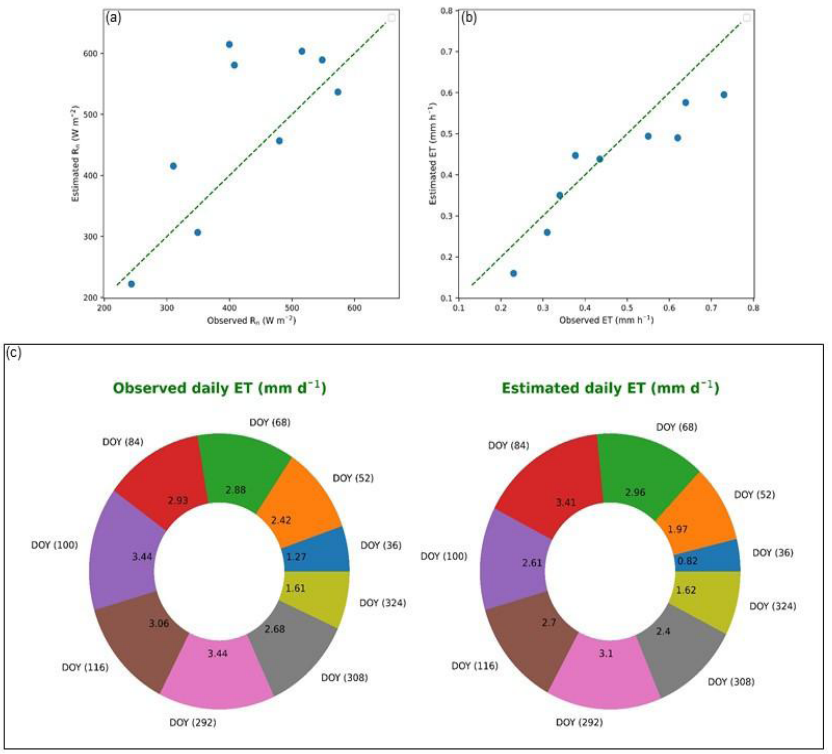

Figure 5. Comparison of estimated net radiation (a), instantaneous evapotranspiration (b) and daily evapotranspiration (c) using Landsat-8 images with the observed net radiation, mean hourly reference evapotranspiration and daily evapotranspiration from EC flux tower data.

With the comparable preliminary results from Landsat-8 images using the T-VI space method, we finally were able to compute ET results. The errors obtained for estimated instantaneous ET and daily ET are comparable with the errors obtained by Pérez et al. (2017) using the T-VI space methodology. A study done by Peng et al. (2013) got 21.7% errors in estimated ET, which is comparable with our results. We obtained around 50% error for two net radiation results but that error has not affected in accuracy of ET estimation very much. This might be because ET estimation using T-VI space method is highly dependent in the accuracy of evaporative fraction calculated from trapezoidal graphical shape. However, due to lack of full EF results from station data, we could not validate all estimated EF results but it can be concluded that accuracy of ET estimation has higher dependency over EF values. Therefore, we should very careful while determining dry edge and wet edge value. Regarding Nepal, there are very limited studies related to evapotranspiration. Research from Amatya et al. (2015), the mean percentage error for the estimated LE was 36.01% and a recent study done by Wasti et al. (2020) estimated daily evapotranspiration using Landsat-8 images for a different part of Nepal with the mean percentage error of 35.07% with the application of Metric Model. Errors obtained in our study for estimated

Conclusion

Major findings in this research have enhanced the understanding of water-scarce agricultural areas, which has suggested for effective irrigation practice during the dry season to solve socio-economic problems like food security risk in Nepal. This research can be concluded as follows:

1) ET results have shown that the T-VI space method using remote sensing data could be an alternative method to estimated ET. The methodology presented in this study has improved the estimated ET accuracy while comparing with past research done in Nepal.

2) The EF obtained from the T-VI space-based trapezoidal shape has shown that waster stress was higher during the winter season and crop growing period (November). Therefore, irrigation water amount should be increased for the dry season.

3) As proved by past results, this T-VI space method is also applicable for drought monitoring along with the understanding of ET. Hence, this research is highly applicable to understand the regional hydrological cycle well.

4) Temporal variation of ET has shown strong relation of ET with NDVI and available solar energy that requires to evaporate the soil moisture available at the moment.

5) Finally, this research has proved the applicability of the T-VI space method over Nepal's agricultural areas.

The southern part of Nepal is a highly productive agricultural area with not enough irrigation water. Therefore, ET estimation is essential to use irrigation water effectively, especially during the dry season. The use of the T-VI space method for ET estimation has been proved a good alternative method, but it is recommended to use cloud removal algorithm in case of a remote sensing-based method relying on satellite images to have the complete temporal understanding of ET and other climatic parameters.

Acknowledgments: This research has been funded by the Second Tibetan Plateau Scientific Expedition and Research (STEP) program (grant no. 2019QZKK0103), National Program on Key Basic Research Project (2018YFC1505701), the Strategic Priority Research Program of Chinese Academy of Sciences (XDA20060101) and the National Natural Science Foundation of China (41830650, 91737205, 91837208).

References

Allen, R. G., L. S. Pereira, D. Raes, and M. Smith, 1998: FAO Irrigation and drainage paper no. 56 - Crop Evapotranspiration.

Allen, R. G., M. Smith, L. S. Pereira, D. Raes, and J. L. Wright, 2004: Revised FAO procedures for calculating evapotranspiration - Irrigation and drainage paper no. 56 with testing in Idaho. Watershed Manag. Oper. Manag. 2000, **105**, 1–10, https://doi.org/10.1061/40499(2000)125.

Allen, R.G., Tasumi,M., Morse,A., Trezza, R.,Wright, J.L., Bastianssen, W., …Robinson, C. W. 2007: Satellite-based energy balance for mapping evapotranspiration with internalized calibration (METRIC)—applications. J. Irrig. Drain. Eng., **133**, 395–406, https://doi.org/10.1061/(asce)0733-9437(2007)133:4(395).

Amatya, P. M., Y. Ma, C. Han, B. Wang, and L. P. Devkota, 2015: Recent trends (2003–2013) of land surface heat fluxes on the southern side of the central Himalayas, Nepal. J. Geophys. Res. Atmos. Res., **175**, 238, https://doi.org/10.1038/175238c0.

Bastiaanssen W.G.M., M. Meneti, R.A. Feddes, and a a M. Holtslag, 1998: A remote sensing surface energy balance algorithm for land (SEBAL). J. Hydrol., **212**–**213**, 198–212.

Batra, N., S. Islam, V. Venturini, G. Bisht, and L. Jiang, 2006: Estimation and comparison of evapotranspiration from MODIS and AVHRR sensors for clear sky days over the Southern Great Plains. Remote Sensing of Environment, **103**, 1–15, https://doi.org/10.1016/j.rse.2006.02.019.

Choi, T., and J. J. Qu, 2017: On-orbit evaporative fraction estimations using a histogram-based triangle

method from Terra MODIS. J. Appl. Remote Sens., **11**, 016038, https://doi.org/10.1117/1.jrs.11.016038.

Choudhury, B. J., N. U. Ahmed, S. B. Idso, R. J. Reginato, and C. S. T. Daughtry, 1994: Relations between evaporation coefficients and vegetation indices studied by model simulations. Remote Sens. Environ., **50**, 1–17, https://doi.org/10.1016/0034-4257(94)90090-6.

Courault, D., B. Seguin, and A. Olioso, 2005: Review on estimation of evapotranspiration from remote sensing data: From empirical to numerical modeling approaches. Irrig. Drain. Syst., **19**, 223–249, https://doi.org/10.1007/s10795-005-5186-0.

Crago, R., and W. Brutsaert, 1996: Daytime evaporation and the self-preservation of the evaporative fraction and the Bowen ratio. J. Hydrol., **178**, 241–255, https://doi.org/10.1016/0022-1694(95)02803-x.

Cristóbal, J., J. C. Jiménez-Muñoz, A. Prakash, C. Mattar, D. Skoković, and J. A. Sobrino, 2018: An improved single-channel method to retrieve land surface temperature from the landsat-8 thermal band. Remote Sens., **10**, https://doi.org/10.3390/rs10030431.

Devkota, N., & Phuyal, R. K. (2016). Climatic impact on wheat production in Terai of Nepal. Journal of Development and Administrative Studies, 23(1-2), 1–22. https://doi.org/10.3126/jodas.v23i1-2.15445

García-Santos, V., J. Cuxart, D. Martínez-Villagrasa, M. A. Jiménez, and G. Simó, 2018: Comparison of three methods for estimating land surface temperature from Landsat 8-TIRS Sensor data. Remote Sens., **10**, 1–13, https://doi.org/10.3390/rs10091450.

Garcia, M., N. Fernández, L. Villagarcía, F. Domingo, J. Puigdefábregas, and I. Sandholt, 2014: Accuracy of the temperature-vegetation dryness index using MODIS under water-limited vs. energy-limited evapotranspiration conditions. Remote Sensing of Environment, **149**, 100–117, https://doi.org/10.1016/j.rse.2014.04.002.

George H. Hargreaves, and Zohrab A. Samani, 1985: Reference crop evapotranspiration from temperature. Appl. Eng. Agric., **1**, 96–99, https://doi.org/10.13031/2013.26773.

Ghorbani, A., J. Karami, N. Olah, G. Bidkhani, and B. Sobhani, 2015: Comparative evaluation of SEBAL and METRIC algorithms for estimation of evapotranspiration (in Persian).

Gordon, S. I., 1980: Utilizing LANDSAT imagery to monitor land-use change: A case study in ohio. Remote Sens. Environ., **9**, 189–196, https://doi.org/10.1016/0034-4257(80)90028-0.

Hamal, K., S. Sharma, N. Khadka, G. G. Haile, B. B. Joshi, T. Xu, and

B. Dawadi, 2020: Assessment of drought impacts on crop yields across Nepal during 1987–2017. Meteorol. Appl., **27**, https://doi.org/10.1002/met.1950.

Hu, X., H. Ren, K. Tansey, Y. Zheng, D. Ghent, X. Liu, and L. Yan, 2019: Agricultural drought monitoring using European Space Agency Sentinel 3A land surface temperature and normalized difference vegetation index imageries. Agric. For. Meteorol., **279**, 107707, https://doi.org/10.1016/j.agrformet.2019.107707.

Huang, J. J., H. Chen, T. Li, E. McBean, and V. P. Singh, 2020: A modified trapezoid framework model for partitioning regional evapotranspiration. Hydrol. Process., 1–17, https://doi.org/10.1002/hyp.13923.

Jiang, L., and S. Islam, 2001: Estimation of surface evaporation map over southern Great Plains using remote sensing data. Water Resour. Res., **37**, 329–340, https://doi.org/10.1029/2000WR900255.

Jimenez-Munoz, J. C., J. Cristobal, J. A. Sobrino, G. Sòria, M. Ninyerola, and X. Pons, 2009: Revision of the single-channel algorithm for land surface temperature retrieval from landsat thermal-infrared data. IEEE Trans. Geosci. Remote Sens., **47**, 339–349, https://doi.org/10.1109/TGRS.2008.2007125.

Karki, R., R. Talchabhadel, J. Aalto, and S. K. Baidya, 2016: New climatic classification of Nepal. Theor. Appl. Climatol., **125**, 799–808, https://doi.org/10.1007/s00704-015-1549-0.

MacDonald, R. B., F. G. Hall, and R. B. Erb, 1975: Use of Landsat Data in a Large Area Crop Inventory Experiment (Lacie). 1–23.

Madugundu, R., K. A. Al-Gaadi, E. K. Tola, A. A. Hassaballa, and V. C. Patil, 2017: Performance of the METRIC model in estimating evapotranspiration fluxes over an irrigated field in Saudi Arabia using Landsat-8 images. Hydrol. Earth Syst. Sci., **21**, 6135–6151, https://doi.org/10.5194/hess-21-6135-2017.

Menon, N., 2009: Rainfall uncertainty and occupational choice in agricultural households of rural Nepal. J. Dev. Stud., **45**, 864–888, https://doi.org/10.1080/00220380902807387.

Minacapilli, M., S. Consoli, D. Vanella, G. Ciraolo, and A. Motisi, 2016: A time domain triangle method approach to estimate actual evapotranspiration: Application in a Mediterranean region using MODIS and MSG-SEVIRI products. Remote Sens. Environ., **174**, 10–23, https://doi.org/10.1016/j.rse.2015.12.018.

Mokhtari, A., H. Noory, F. Pourshakouri, P. Haghighatmehr, Y. Afrasiabian, M. Razavi, F. Fereydooni, and A. Sadeghi Naeni, 2019: Calculating potential evapotranspiration and

single crop coefficient based on energy balance equation using Landsat 8 and Sentinel-2. ISPRS J. Photogramm. Remote Sens., **154**, 231–245, https://doi.org/10.1016/j.isprsjprs.2019.06.011.

Oh, J. W., J. Ngarambe, P. N. Duhirwe, G. Y. Yun, and M. Santamouris, 2020: Using deep-learning to forecast the magnitude and characteristics of urban heat island in Seoul Korea. Sci. Rep., **10**, 1–13, https://doi.org/10.1038/s41598-020-60632-z.

Oki, T., and S. Kanae, 2006: Global hydrological cycles and world water resources. Science (80-.)., **313**, 1068–1072, https://doi.org/10.1126/science.1128845.

Paudel, M. N., 2016: Prospects and Limitations of agriculture industrialization in Nepal. Agron. J. Nepal, **4**, 38–63, https://doi.org/10.3126/ajn.v4i0.15515.

Peng, J., Y. Liu, X. Zhao, and A. Loew, 2013: Estimation of evapotranspiration from MODIS TOA radiances in the Poyang Lake basin, China. Hydrol. Earth Syst. Sci., **17**, 1431–1444, https://doi.org/10.5194/hess-17-1431-2013.

Pérez, J. Á. M., S. G. García-Galiano, B. Martin-Gorriz, and A. Baille, 2017: Satellite-based method for estimating the spatial distribution of crop evapotranspiration: Sensitivity to the priestley-taylor coefficient. Remote Sens., **9**, https://doi.org/10.3390/rs9060611.

Price, J. C., 1990: U sing Spatial Context in Satellite Data to Infer Regional Scale Evapotranspiration. IEEE Trans. Geosci. Remote Sens., **28**, 940–948, https://doi.org/10.1109/36.58983.

Priestley, C. H. B., and R. J. Taylor, 1972: On the Assessment of Surface Heat Flux and evaporation using large-scale parameters. *Monthly Weather Review, **100**, 81–92*, https://doi.org/10.1175/1520-0493(1972)100<0081:OTAOSH>2.3.CO;2.

Reyes-gonz, A., J. Kjaersgaard, T. Trooien, D. G. Reta-s, I. S. Juan, P. Preciado-rangel, and M. Fortis-hern, 2019: Comparison of leaf area index , surface temperature , METRIC Model and In Situ Measurements. Sensor, **19**, 2–21.

Saitta, D., D. Vanella, J. M. Ramírez-Cuesta, G. Longo-Minnolo, F. Ferlito, and S. Consoli, 2020: Comparison of orange orchard evapotranspiration by eddy covariance, sap flow, and FAO-56 methods under different irrigation strategies. J. Irrig. Drain. Eng., **146**, 05020002, https://doi.org/10.1061/(asce)ir.1943-4774.0001479.

Shrestha, N., D. Raes, E. Vanuytrecht, and S. K. Sah, 2013: Cereal yield stabilization in Terai (Nepal) by water and soil fertility management modeling. Agric. Water Manag., **122**,

53–62, https://doi.org/10.1016/j.agwat.2013.03.003.

Subba, S., Y. Ma, and W. Ma, 2019: Spatial and temporal analysis of precipitation extremities of Eastern Nepal in the last two decades (1997–2016). J. Geophys. Res. Atmos., **124**, 7523–7539, https://doi.org/10.1029/2019JD030639.

Sun, H., 2016: Two-Stage Trapezoid: A New Interpretation of the land surface temperature and fractional vegetation coverage space. IEEE J. Sel. Top. Appl. Earth Obs. Remote Sens., **9**, 336–346, https://doi.org/10.1109/JSTARS.2015.2500605.

Tang, R., Z. L. Li, and B. Tang, 2010: An application of the Ts-VI triangle method with enhanced edges determination for evapotranspiration estimation from MODIS data in arid and semi-arid regions: Implementation and validation. Remote Sens. Environ., **114**, 540–551, https://doi.org/10.1016/j.rse.2009.10.012.

Tanguy, M., A. Baille, M. M. González-Real, C. Lloyd, B. Cappelaere, L. Kergoat, and J. M. Cohard, 2012: A new parameterisation scheme of ground heat flux for land surface flux retrieval from remote sensing information. J. Hydrol., **454**–**455**, 113–122, https://doi.org/10.1016/j.jhydrol.2012.06.002.

Walter, I. A., and Coauthors, 2004: ASCE's standardized reference evapotranspiration equation. Watershed Manag. Oper. Manag. 2000, **105**, https://doi.org/10.1061/40499(2000)126.

Wasti, S., W. Ma, and Y. Ma, 2020: Estimation of land surface evapotranspiration using the METRIC model in Nepal. Atmos. Ocean. Sci. Lett., **13**, 509–517, https://doi.org/10.1080/16742834.2020.1824984.

Yamazaki, D., S. Kanae, H. Kim, and T. Oki, 2011: A physically based description of floodplain inundation dynamics in a global river routing model. Water Resour. Res., **47**, 1–21, https://doi.org/10.1029/2010WR009726.

Yu, X., X. Guo, and Z. Wu, 2014: Land surface temperature retrieval from landsat 8 TIRS-comparison between radiative transfer equation-based method, split window algorithm and single channel method. Remote Sens., **6**, 9829–9852, https://doi.org/10.3390/rs6109829.

Zhu, W., S. Jia, U. Lall, Y. Cheng, and P. Gentine, 2020: An observation-driven optimization method for continuous estimation of evaporative fraction over large heterogeneous areas. Remote Sens. Environ., **247**, 111887, https://doi.org/10.1016/j.rse.2020.111887.